Laser cladding of Ni based powder on a Cu-Ni-Al glassmold: Influence of the process parameters on bonding quality and coating geometry

F. Bourahima, A. L. Helbert, M. Rege, V. Ji, D. Solas, T. Baudin

Journal of Alloys and Compounds 771 (2019) 1018–1028

Contents lists available at ScienceDirect

Journal of Alloys and Compounds

journal homepage: http://www.elsevier.com/locate/jalcom

Review

Laser cladding of Ni based powder on a Cu-Ni-Al glassmold: Influence of the process parameters on bonding quality and coating geometry

F. Bourahima [a, b], A.L. Helbert [b, *], M. Rege [a], V. Ji [b], D. Solas [b], T. Baudin [b]

[a] Etablissements Chpolansky, 91 462, Marcoussis, France
[b] ICMMO, SP2M, Univ. Paris-Sud, Université Paris-Saclay, UMR CNRS 8182, Bât.410, 91405, ORSAY, France

ARTICLE INFO

Article history:
Received 16 May 2018
Received in revised form
28 August 2018
Accepted 1 September 2018
Available online 3 September 2018

Keywords:
Laser cladding
ANOVA
Bonding
Power attenuation
Scanning speed

ABSTRACT

Laser cladding of a Ni based powder on cupro-nickel-aluminum (Cu-Ni-Al) substrate was performed with a 4 kW continuous laser. The Cu-Ni-Al alloy is used for its thermal properties in glass mold industry. The role of the Ni based alloy clad is to protect the mold without affecting its thermal properties by limiting the heat-affected zone. The objective of this research is to produce a well bonded Ni based melted powder without pores or cracks and with a very small dilution zone on a non-planar surface (curved section). The impact of the process parameters such as laser power, scanning speed and powder feeding rate on the coating geometry was investigated with an experimental design technique analysis using the ANOVA (Analysis of variance) method. It was used to determine and represent the influence of each process parameter on the coating geometry (width, height) and the bonding quality. This ANOVA analysis led to a parameter combination to optimize the bonding quality between the Ni coating and the Cu-Ni-Al substrate taking into account the industrial geometrical constraints. More, an analytical calculation allowed to estimate the power necessary for bonding as a function of laser scanning speed and powder feeding rate.

Contents

1. Introduction

The process of glass bottle production consists in pouring viscous glass at a range of temperature from 700 to 1200 °C in Cu-Ni-Al glass molds. Those glass molds play the role of thermal exchangers during the glass bottle production. During molding, abrasion and corrosion can appear on sensitive parts of the mold (neck and ring) in contact with the viscous glass. It is essential to modify the mold surface properties in order to extend its service

* Corresponding author.
E-mail address: anne-laure.helbert@u-psud.fr (A.L. Helbert).

https://doi.org/10.1016/j.jallcom.2018.09.004
0925-8388/

life.

Laser cladding is an advanced surfacing method [1] used to produce well bonded high-performance materials, fully dense coatings without interfering on their thermal properties. Indeed, many studies reported that laser cladding allows to obtain very low heat-affected zone compared to other surfacing technics like Plasma Transferred Arc [2]. Nevertheless, a local chemical dilution between the melted powder and the melted substrate during laser cladding is necessary since the bonding coating/substrate is directly linked to the existence and thickness of this dilution zone [3]. The dilution is defined as the ratio of cladding depth to the sum of cladding height and cladding depth.

Many analyses have been done to investigate the influence of the process parameters on the dilution for a plane surface deposition. Ming et al. [4] have reported, for laser cladding of Ni based powders on an AISI 1020 substrate (steel), that the dilution increases with the increase of the scanning speed and the decrease of the powder feeding rate (PFR). Moosa et al. [5] found the same trend during laser cladding of Ni-10 wt%Al and Ni-30 wt% Al on Inconel 617 substrate. In fact, they showed that dilution depends both on laser scanning speed and on chemical composition of involved materials. According to the authors, at high speed, the powder density available for cladding is low, so the cladding height (H) will be smaller and the dilution will increase since more power (P) is then available for the substrate melting.

Sun and Hao [6] have observed the opposite dilution behavior with speed, for laser cladding of Ti6Al4V powder on a substrate with the same compound. In fact, after an ANOVA analysis they have found that the dilution decreased with high scanning speed. According to these authors, at high speed, the powder density for cladding is low, this will lead to a less molten penetration and so the dilution will be lower. So, in Refs. [4] and [6], the same argument (based on the energy and powder density) is used to explain two opposite behaviors. As a conclusion, the scanning speed effect on dilution and bonding remains poorly understood and will be investigated in this study.

In the present work, different powers will be calculated within the laser cladding process. Especially, the power that reaches the substrate, at the origin of a strengthened bonding, will be estimated subtracting an attenuated power due to particles shadow as well as the power necessary for powder melting.

Beside the bonding management, laser cladding parameters have to be adjusted to guaranty the clad geometry imposed by glass mold industry so that cladded molds can be machined later on, in order to obtain perfect glass surfaces.

The geometrical characteristics of the coating have interested some researchers concerning plane surface deposition. Ming et al. [4] have found out that clad height increases when the PFR increases and the scanning speed decreases. It can be explained by the fact that at high speed, the powder density is low and so H will be lower. The same observation has been done with the coating width (W).

De Oliveira et al. [7] have observed that laser scanning speed and the PFR have more influence on H and W than the laser power itself, for Ni based powder cladding on C45 substrate (low-alloyed steel). The same observation has been made by Ocelick et al. [8] after laser cladding of Co-based powder on cast iron.

Peyre et al. [9] have explained that the clad height depends on the PFR and scanning speed (v) as follows:

$$H = \frac{D_m^*}{\rho}.\frac{d}{v} \quad (1)$$

With H the deposited height [m], D_m^* the local surface PFR [$\frac{kg}{m^2 s}$] corresponding to the PFR divided by the laser spot surface, d the laser spot diameter [m], ρ the Ni density [$\frac{kg}{m^3}$], and v the laser scanning speed [$\frac{m}{s}$].

In the literature, the combined effects of the different laser process parameters on bonding and clad geometry are not really studied and more, all the presented works deal with deposition on plane surfaces while the mold surface of this present study is curved.

In this paper, a statistical analysis using the ANOVA (Analysis of variance) method and an experimental study of the influence of laser cladding parameters on coating bonding and geometry is presented. The aim is to determine the individual and combined effects of each of the main parameters which are scanning speed, PFR and laser power. An optimization of the parameters is expected to favor the best bonding on a complex substrate geometry respecting the height (H) and width (W) industrial ranges.

2. Material and experimental techniques

In this work, a 4 KW Nd: YAG laser with a wavelength of 1033 nm is used. Laser surfacing technology consists in depositing an amount of melted based powder. An optical fiber with a diameter of 600 μm was used for guiding the beam. The focal length is 200 mm. The chemical compositions of the powder and the substrate used in the present paper are listed in Table 1. The material properties of the powder and the substrate are given in Table 2.

A half of the Cu-Ni-Al mold of the bottle ring is presented in Fig. 1 after cladding. Fig. 2 describes a typical cross section after laser cladding of the mold curved surface. To be characterized, the sample is coated with a conductive resin (Polyfast), mechanically polished on SIC papers and polished using diamond suspensions until 1 μm for optical microscopy analysis.

Fig. 2 describes the different bonding qualities between the nickel coating and the substrate that can be experimentally obtained. Fig. 2a shows a perfect bonding whereas in Fig. 2b and c the bonding is partial or not obtained, respectively. The height H and the width W of the deposited material are measured as shown in Fig. 2d where H is taken along the powder projection axis.

To study the influence of the process parameters on the coating geometry and the bonding quality after laser cladding, a Taguchi design of experiment with a table of 25 tests has been used [10]. 3 factors have been taken into account: the laser power (W), the scanning speed (mm/s) and the PFR (g/min). Each factor counts 5 different values. Among the obtained results, 16 tests were selected with spot diameter fixed from 3 to 4 mm because a spot size lower than 3 mm and higher than 4 mm does not allow to obtain the wanted coating geometry. Let us note that the intended ranges of clad height and width are 1.8–2.5 mm and 3.5–4.5 mm, respectively.

3. ANOVA calculation

The obtained data were statistically analyzed by an ANOVA method using Design Expert V9.0 [6]. The purpose is to optimize the process parameters to guaranty a good bonding while respecting the imposed industrial values of H and W chosen in order to allow a further machining of the coated mold. The central composite design (CCD) was used [11]. The main process parameters are the laser power P, the scanning speed v and the powder feeding rate PFR. The design of experiment is done with the parameters given in Table 3. The bonding is described as a binary value: 1 for bonding and 0 when there is either no bonding or partial bonding.

Each factor varies over five levels from the high level (+1) to the low level (−1). The center point is zero. The two-outer points alpha

Table 1
Chemical composition of the substrate and powder.

Chemical elements (wt%)	Fe	Mn	Al	Ni	Zn	Pb	Sn	Si	Cu	B	Cr	C
Cu-Ni-Al	<1	0.5	8.5	15	8	<0.1	0.15	1	Bal	–	–	–
Ni based powder	1	0.1	–	Bal	–	–	–	2.5	–	1.7	0.3	0.5

Table 2
Material properties of the substrate and powder.

	Density ρ (kg/m^3)	Thermal fusion T_f (°K)	Heat capacity C_p (J/kg/°K)	Latent heat L_f (J/kg)
Cu-Ni-Al substrate	7400	1323	377	220000
Ni based powder	8900	1728	440	298000

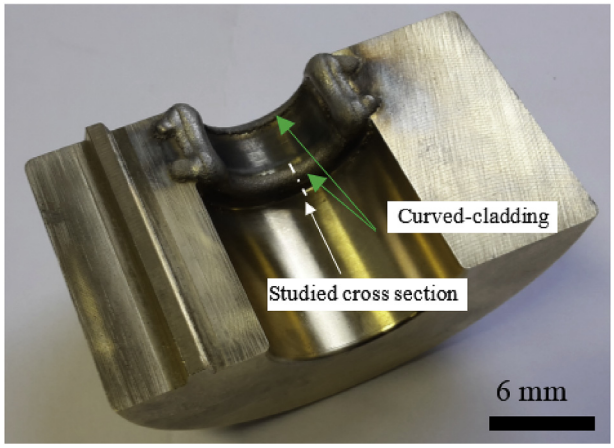

Fig. 1. Mold after Ni-laser cladding.

(the axial points of the spherical design) are equal to ± 1.414. The Response Surface Method (RSM) [11] is a regression method giving the relation between the response y and the process parameters x. It is a second order equation:

$$y = f(x_1, x_2) + \varepsilon = x_0 + \sum_{j=1}^{k} \alpha_j x_j + \sum_{j=1}^{k} \alpha_{jj} x_j^2 + \sum_{i<j} \sum_{j=2}^{k} \alpha_{ij} x_i x_j + \varepsilon \quad (2)$$

where y is the predicted response (bonding, height and width), x_0 is a constant value, α_j is the jth linear coefficient, α_{jj} is the jth quadratic coefficient, α_{ij} is the ith interaction coefficient, x_j is the independent variable (power, scanning speed and PFR), k is the number of factors and ε is the associated error.

Tables 4–6 present the results of the ANOVA analysis which confirm that the three mathematical models for the bonding, width and height are significant since p-values <0.05 (which indicates

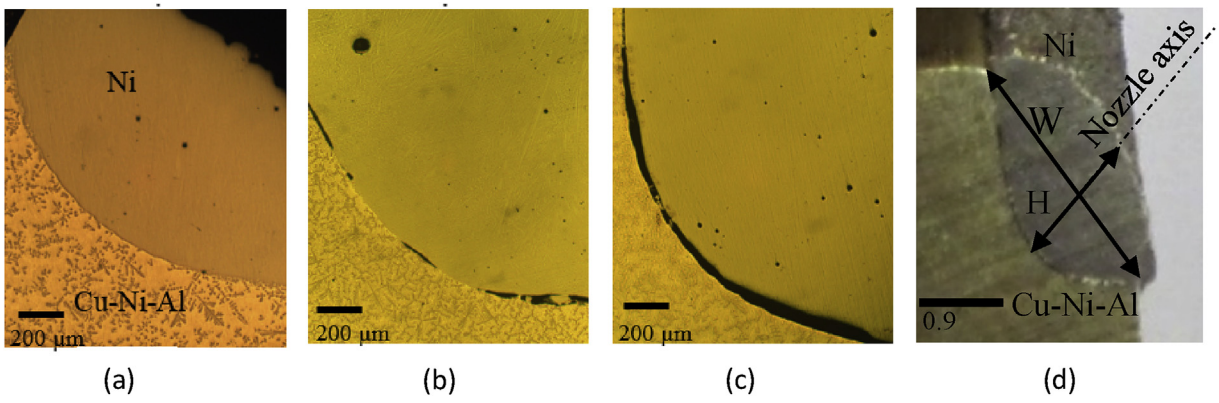

Fig. 2. Criteria of bonding (a) perfect bonding with the following parameters P = 2800 W, v = 8.5 mm/s and PFR = 24.5 g/min, (b) partial bonding with P = 2400 W, v = 4.5 mm/s and PFR = 26.5 g/min and (c) no bonding with P = 3000 W, v = 6.5 mm/s, PFR = 24.5 g/min and spot size = 5 mm and coating geometry features (d) height (H) and width (W) of the clad.

Table 3
Ranges and designations of the studied process factors.

	Power (W)	Speed (mm/s)	Powder feeding rate (g/min)
Designation	P	v	PFR
High alpha level (1,414)	3200	10	32.5
High level (+1)	3000	8.5	30.5
Zero level (0)	2800	6.5	28.5
Low level (−1)	2600	4.5	26.5
Low alpha level (−1414)	2400	2.5	24.5
Variation range	200	2.0	2.0

Table 4
ANOVA analysis of bonding. Parameters (and corresponding values) are in italics.

Source	Sum of Squares	df	Mean Square	F Value	p-value Prob > F	
Model	3.700	9	0.410	77.230	<0.0001	significant
P-Power	*0.690*	*1*	*0.690*	*129.250*	*< 0.0001*	
PFR-Powder Feeding Rate	*0.430*	*1*	*0.430*	*81.040*	*< 0.0001*	
v-Scanning Speed	*0.830*	*1*	*0.830*	*155.680*	*< 0.0001*	
PPFR	*0.025*	*1*	*0.025*	*4.720*	*0.0549*	
Pv	*0.440*	*1*	*0.440*	*82.970*	*< 0.0001*	
PFRv	*0.330*	*1*	*0.330*	*61.250*	*< 0.0001*	
P^2	*0.030*	*1*	*0.030*	*5.680*	*0.038*	
PFR^2	*5.162E-003*	*1*	*5.162E-003*	*0.970*	*0.348*	
v^2	*0.028*	*1*	*0.028*	*5.270*	*0.045*	
Residual	0.053	10	5.318E-003			
Cor Total	3.750	19				

Table 5
ANOVA analysis of width.

Source	Sum of Squares	df	Mean Square	F Value	p-value Prob > F	
Model	5.580	9	0.620	7.630	0.033	significant
P-Power	*3.224E-004*	*1*	*3.224E-004*	*3.964E-003*	*0.953*	
PFR-Powder Feeding Rate	*0.016*	*1*	*0.016*	*0.200*	*0.681*	
v-Scanning Speed	*1.580*	*1*	*1.580*	*19.370*	*0.012*	
PPFR	*8.127E-003*	*1*	*8.127E-003*	*0.100*	*0.768*	
Pv	*1.375E-004*	*1*	*1.375E-004*	*1.691E-003*	*0.969*	
PFRv	*0.014*	*1*	*0.014*	*0.180*	*0.695*	
P^2	*0.270*	*1*	*0.270*	*3.330*	*0.142*	
PFR^2	*0.030*	*1*	*0.030*	*0.370*	*0.578*	
v^2	*0.190*	*1*	*0.190*	*2.390*	*0.197*	
Residual	0.330	4	0.081			
Cor Total	5.910	13				

Table 6
ANOVA analysis of height.

Source	Sum of Squares	Df	Mean Square	F Value	p-value Prob > F	
Model	24.190	9	2.690	25.690	0.0004	significant
P-Power	*0.066*	*1*	*0.066*	*0.630*	*0.456*	
PFR-Powder Feeding Rate	*9.114E-003*	*1*	*9.114E-003*	*0.0870*	*0.778*	
v-Scanning Speed	*11.120*	*1*	*11.120*	*106.310*	*< 0.0001*	
PPFR	*0.055*	*1*	*0.055*	*0.530*	*0.496*	
Pv	*0.011*	*1*	*0.011*	*0.110*	*0.753*	
PFRv	*0.016*	*1*	*0.016*	*0.150*	*0.712*	
P^2	*0.110*	*1*	*0.110*	*1.090*	*0.336*	
PFR^2	*0.020*	*1*	*0.020*	*0.190*	*0.679*	
v^2	*0.600*	*1*	*0.600*	*5.750*	*0.053*	
Residual	0.630	6	0.100			
Cor Total	24.820	15				

less than 5% chance that a F-value could occur due to noise) and the F-values, especially for bonding and height, are high [7]. Results in Table 4 show that the three parameters have an equivalent influence on bonding. Besides, the parameters that are coupled to the scanning speed have a high impact on the bonding. Concerning the width (Table 5), the power (P) has a very low impact compared to the other two parameters, and the scanning speed (v) has the highest influence. Among the coupled effects, parameter PFRv has the largest effect on width. In Table 6, it can be seen that scanning speed has the major effect on H. The coupled parameters have equivalent impacts.

Using this ANOVA model, the following second order equations for the bonding (B), width (W) and height (H) are the following, Eqs. (3)–(5), respectively:

$$B = 4.57 + 4.29.10^{-3}P - 0.76PFR + 0.17v + 2.23.10^{-4}P.PFR - 5.32.10^{-4}P.v + 0.055PFR.v \\ -1.04.10^{-6}P^2 - 6.27.10^{-3}PFR^2 - 9.1.10^{-3}v^2 \quad (3)$$

$$W = 92.56 - 0.04\,P - 1.96PFR - 1.17v + 1.38.10^{-4}\,P.PFR + 4.67.10^{-5}P.v + 0.05PFR.v \\ +6.29.10^{-6}P^2 + 0.02PFR^2 - 0.04v^2 \quad (4)$$

$$H = 21.65 - 7.4.10^{-3}P - 0.24PFR - 1.49v - 2.9.10^{-4}P.PFR - 3.3.10^{-4}P.v + 0.03PFR.v \\ +3.4.10^{-6}P^2 + 0.01PFR^2 + 0.06v^2 \quad (5)$$

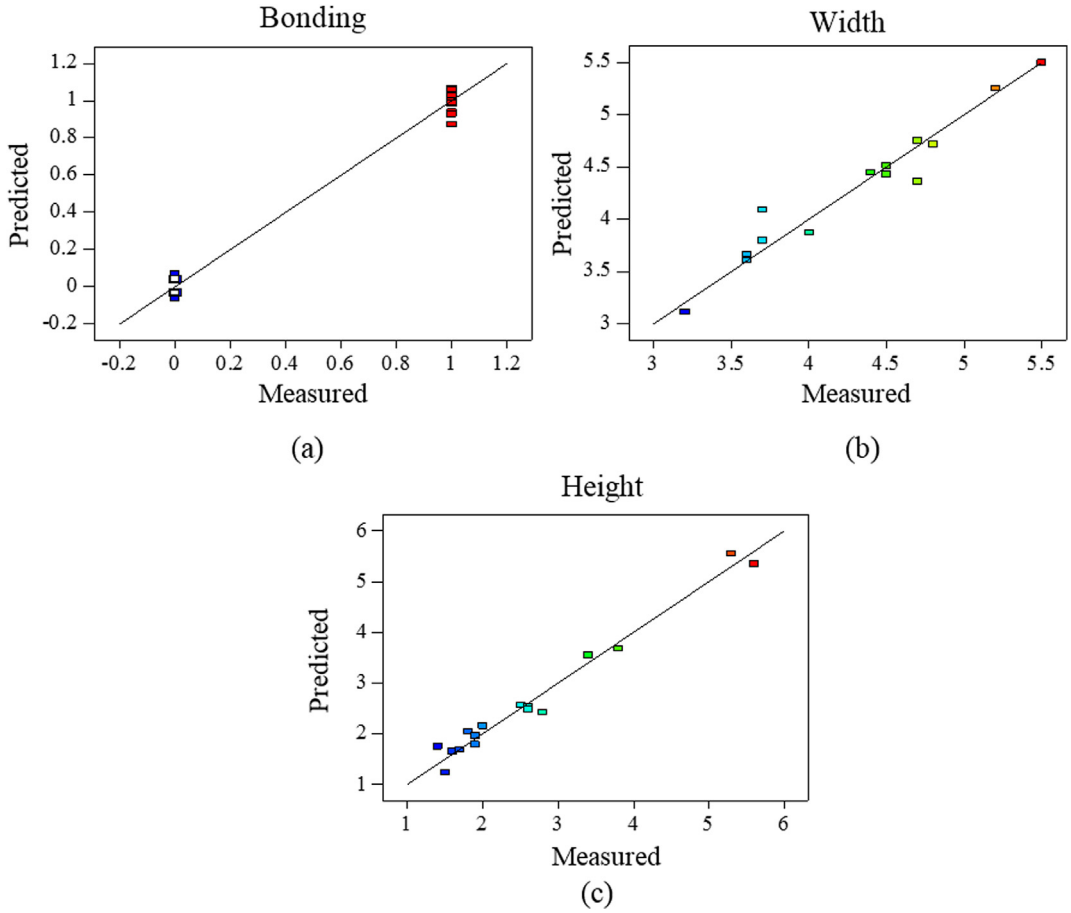

Fig. 3. ANOVA predicted vs. measured values of (a) bonding, (b) width and (c) height.

Fig. 3 presents the comparison between the ANOVA calculated values of bonding, H and W and the experimental ones.

Fig. 3 allows us to observe that the calculated values are very close to the experimental ones. Then, the adequacy of developed models is verified for the bonding, the height and width. In fact, the respective values of predicted R^2 are 0.986 for the bonding, 0.975 for the height and 0.945 for the width.

3.1. The bonding

Fig. 4 shows the influence of the process parameters on the bonding. For each 2D representation, a parameter has been fixed at the value usually used by the CHPOLANSKY Company (P = 2800 W, PFR = 28.5 g/min and v = 6.5 mm/s). It can be observed in Fig. 4 that the bonding is possible from 3100 to 3200 W whatever the scanning speed. For lowest powers, bonding is possible only if scanning speed is high. According to Fig. 4b, for a given power, the increase of PFR decreases the bonding. Fig. 4c shows that a high scanning speed (more than 7 mm/s) allows bonding whatever the PFR value. As it has been observed by Ming et al. [4] and Sun and Hao [6], the increase of PFR and the decrease of scanning speed lead to a high powder density that will absorb the input power energy. So, less power is then available for the substrate local fusion. Thus, depending on the process parameters, a lack of bonding can be observed. Also, bonding increases with the power. This is because at high power favors both powder and substrate melting. Then, from these first results, it appears that the three process parameters have a very important role for the bonding.

Apart from the bonding quality between the nickel deposit and the substrate, it is necessary to respect imposed values of width (from 3.5 to 4.5 mm) and height (from 1.8 to 2.5 mm) for the coating. Indeed, a too small Ni coating induces a material lack after mold machining and a too large coating represents a waste of material.

3.2. The width

To obtain the wanted values of width (pink delimited areas in Fig. 5), it is possible to use power from 2600 to 3000 W if some restriction of PFR and scanning speed are respected: a scanning speed higher than about 7 mm/s (Fig. 5a) and a PFR higher than about 26.5 g/min (Fig. 5b). Fig. 5c shows that the scanning speed range included between 7 and 8.5 mm/s allows to obtain the imposed W values whatever the PFR.

3.3. The height

As for W, Fig. 6a and c indicate that H decreases while scanning speed increases. Fig. 6b shows that neither PFR nor power has a significant influence on H.

This can be explained by the fact that when the speed is increased, less powder is available for the fusion and so the height will be lower. This has been observed by Peyre et al. [9]. Their proposed (Eq. (1)) allows to calculate the clad height as a function

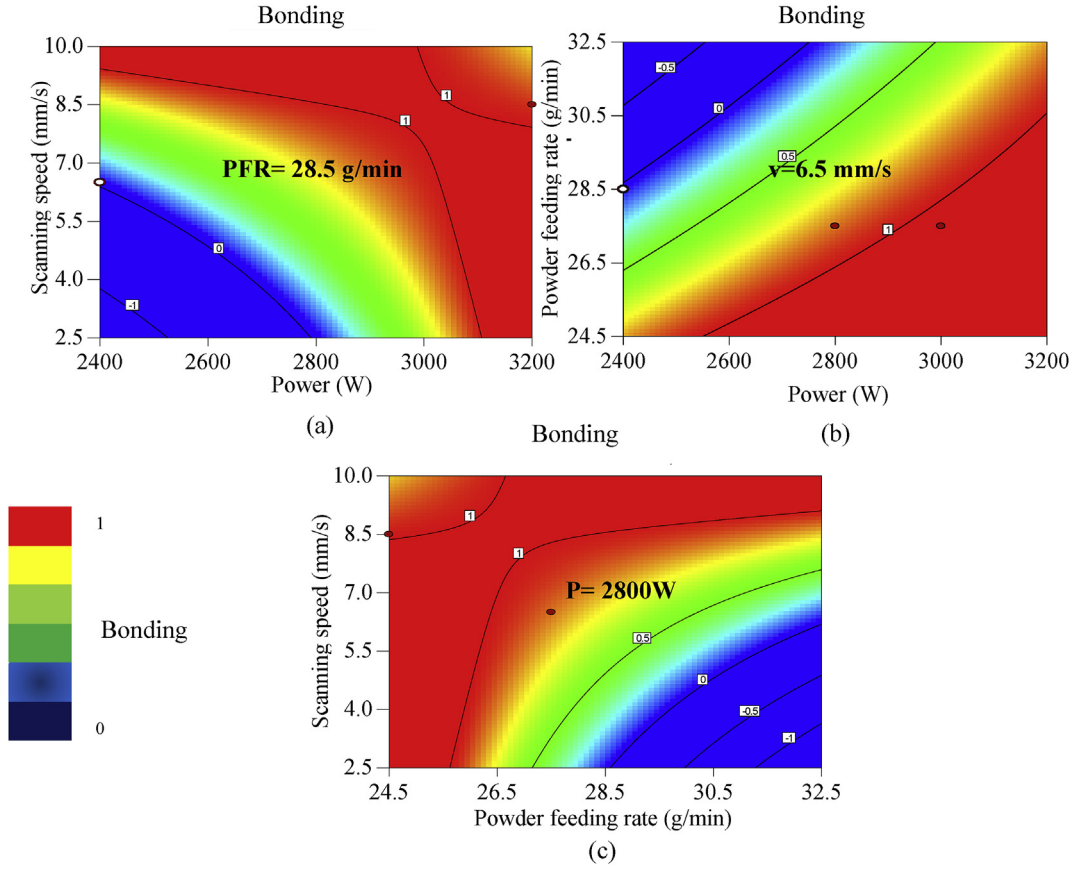

Fig. 4. Bonding evolution with (a) the scanning speed (mm/s) and the power (W) for a fixed value of PFR at 28.5 g/min (b) the PFR (g/min) and the power (W) for a fixed value of scanning speed at 6.5 mm/s and (c) the scanning speed (mm/s) and the PFR (g/min) for a fixed value of power at 2800 W.

of the laser scanning speed that can be compared to the present ANOVA height predictions (Fig. 6).

Fig. 7 allows us to observe that the ANOVA calculation of height is very close to that calculated from Eq. (1) [9], which means that the statistical modelling is accurate. It can be seen that to obtain the wanted height (between 1.8 and 2.5 mm delimited by continuous blue lines), at the conditions of calculation described here, a speed between 6.5 and 8.5 mm/s has to be respected.

4. Discussion

4.1. Optimization

One of the aims of this study was to obtain a good Ni coating bonding respecting the industrial geometry limitations. The optimized domains, corresponding to sets of parameters leading to bonding and where the ranges of height and width, are then extracted from ANOVA analysis and are delimitated by blue dotted lines in Fig. 8.

Note that for the selected representation at v = 6.5 mm/s, the optimized domain is restricted to a limited zone. Nevertheless, a large range of parameters is available to get a successful cladding. A set of parameters is then chosen inside this optimized area as: power 2800 W, scanning speed 8.5 mm/s and PFR of 27.5 g/min for cladding validation. The ANOVA predicted geometry associated with a good bonding is experimentally verified as presented in Fig. 9 (W = 3.7 ± 0.02 mm and H = 1.9 ± 0.2 mm).

4.2. The bonding

The bonding quality is obviously linked to the laser power that effectively reaches the substrate (mold) to improve the molten penetration and thus create a dilution area. In order to calculate this power, Tabernero et al. [12] have described the phenomenon of attenuation of the incident energy because of the powder during laser cladding. This attenuation is represented by the attenuation factor K_{att}, dimensionless. They assume that this power attenuation is proportional to the shadow generated by the particles of powder during the interaction time with the laser beam. The shadowed power (P_{shad}) is then calculated as follows:

$$P_{shad} = K_{att}.P_i \tag{6}$$

With P_i the initial power [W] and K_{att} the attenuation factor such as:

$$K_{att} = \alpha \frac{3.D_m^*}{4.R_{particle}\cdot\rho}.\frac{\Delta Z}{v_{z\_particle}} \tag{7}$$

With D_m^* the mass flow of powder particles over the laser beam surface $\left[\frac{kg}{m^2 s}\right]$, Δz the distance over which powder particles are interacting with the laser beam [m], $R_{particle}$ the radius of a powder particle [m], $v_{z\_particle}$ the particle speed along the nozzle axis $[\frac{m}{s}]$. As defined by the authors [12], α is a material attenuation factor that includes physical phenomena neglected by the model (scattering effect, generation of plasma…). In order to do this calculation (Eq. (7)), a set of hypotheses has been done: the attenuation is

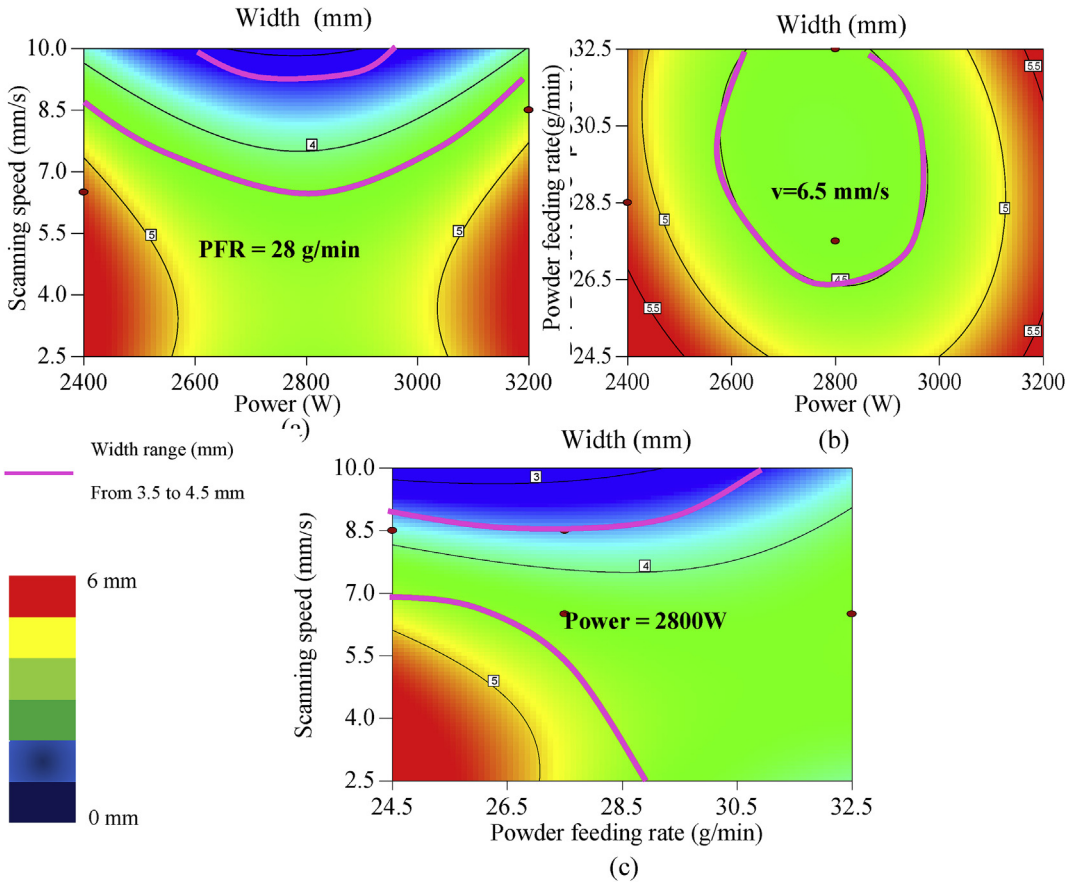

Fig. 5. Width evolution with (a) the scanning speed (mm/s) and the power (W) for a fixed value of PFR at 28.5 g/min, (b) the PFR (g/min) and the power (W) for a fixed value of scanning speed at 6.5 mm/s and (c) the scanning speed (mm/s) and the PFR (g/min) for a fixed value of power at 2800 W. The attended width range is delimited by pink lines. (For interpretation of the references to colour in this figure legend, the reader is referred to the Web version of this article.)

independent from the power, the particles are spherical, powder and power distributions are Gaussian. The attenuated power, available after the laser beam interaction with the powder particles, is then P_{att}, such as:

$$P_{att} = P_i - P_{shad} = P_i(1 - K_{att}) \tag{8}$$

P_{att} is calculated using the K_{att} attenuation factor (Eq. (7)). In order to determine the α factor, a measurement of the attenuated power during laser cladding has been carried out with a power meter placed under an optically neutral glass to protect it from the powder injected. During the test, an air flow was injected horizontally in order to deflect the projected powder. As an example, for an incident measured power of 1916 W, the measured attenuated power was 1498 W for a PFR of 28.5 g/min. The experiment power has been limited to 2000W to avoid the neutral glass damage. This led to adjust the α coefficient at a value of 6 (this result is in accordance with literature [12]). If α is equal to 1, the attenuation is only due to particle shadow. The present value of 6 indicates that other phenomena (scattering effect, generation of plasma…) also contribute to the power attenuation.

Fig. 10 shows the attenuated power calculated from Eq. (8) as a function of PFR for a 2800 W incident laser power in the range of PFR used in the present study. It is seen that the K_{att} factor varies from about 20% to 25%.

It is important to note that a part of the shadowed power is reflected and another one is absorbed by the powder particles, P_{abs} [13]. This last one contributes to heat the powder [9]. The usual absorptivity of the Ni based powder under a Nd:YAG irradiation is about $A_p = 0.3$ [14]. So, the power absorbed by the powder particles is then equal to $P_{abs} = A_p.P_{shad}$ and the associated temperature increase is:

$$\Delta T = T_{shad} - T_o = \frac{P_{abs} \cdot \frac{\Delta z}{v_{z\_particle}}}{N_p . m_p . C_p} \tag{9}$$

T_0 [K] is the ambient temperature and T_{shad} [K] is the temperature reached by the particles due to the shadow process within the interaction volume. Δz and $v_{z\_particle}$ were defined Eq. (7). m_p is the mass of a powder particle [kg], N_p is the number of particles in the interaction volume with the laser beam and is calculated as follows:

$$N_p = \frac{D_m^* \cdot \frac{\Delta z}{v_{z\_particle}}}{\rho \cdot V_{particle}} \tag{10}$$

Where $V_{particle}$ is the volume of one particle [m^3].

As an example, using the optimized process parameters defined in section 4.1, T_{shad} reaches 600 K. This temperature is low compared to the melting point 1728 K. The attenuated power that remains after the shadow process is then partially used to heat and melt the powder. This part of power, P_m, is determined by Eq. (11):

$$P_m = E.v \tag{11}$$

with E [$\frac{J}{mm}$] the linear energy to melt the Ni particles and v the laser scanning speed [$\frac{mm}{s}$].

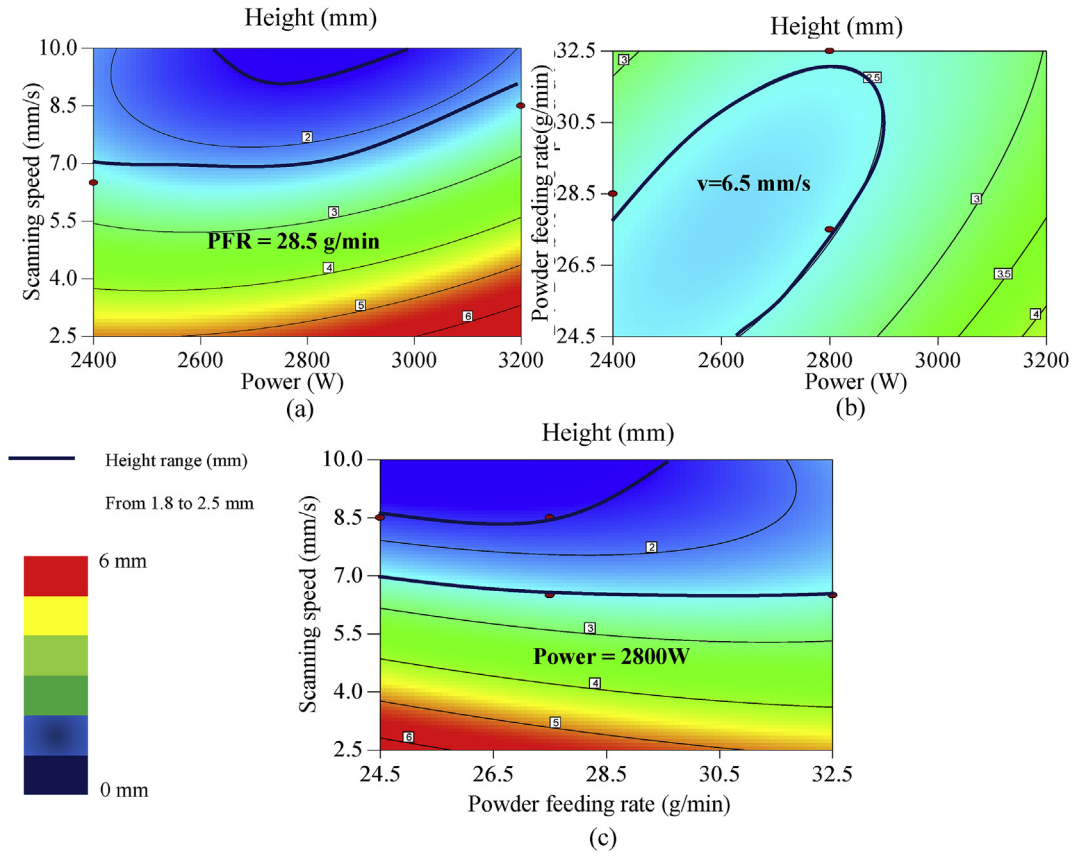

Fig. 6. Height evolution with (a) the scanning speed (mm/s) and the power (W) for a fixed value of PFR at 28.5 g/min, (b) the PFR (g/min) and the power (W) for a fixed value of scanning speed at 6.5 mm/s and (c) the scanning speed (mm/s) and the PFR (g/min) for a fixed value of power at 2800 W. The attended height range is delimited by blue lines. (For interpretation of the references to colour in this figure legend, the reader is referred to the Web version of this article.)

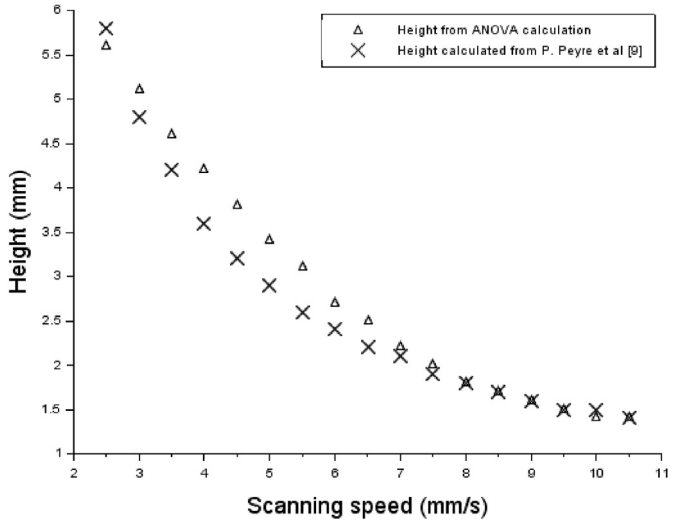

Fig. 7. Influence of the scanning speed on the height for 2800 W and PFR of 27.5 g/min: comparison of ANOVA with Eq. (1) [9].

The linear energy depends on the quantity of powder to be melted which constitutes the clad. The clad section (A) (Fig. 2) evolves with the scanning speed and has been obtained from the ANOVA model assuming that A = 0.66*H*W after a comparison with experimental values. For given laser power and PFR, the heat equation with a change of state is given as follows (Table 2) [14]:

$$E = \rho A\left(C_p \Delta T + L_f\right) \tag{12}$$

With $\Delta T = (T_m - T_{shad})$ where $T_m = 1728$ K is the Ni melting temperature and T_{shad} the initial temperature after the shadow effect. P_m has been calculated and varies from 200 W to 400 W depending on the scanning speed and the PFR.

It can be assumed, in first approximation that P_{sub}, which finally reaches the substrate surface, is:

$$P_{sub} = P_{att} - P_m \tag{13}$$

It is lastly possible to calculate P_{sub} at the substrate surface. An example of the evolution of P_{sub} as a function of PFR is given in Fig. 11a for the optimized power (2800 W) and scanning speed 8.5 mm/s. It is observed that P_{sub} slightly decreases with PFR in this range of PFR. This is in agreement with the fact that a high quantity of powder consumes a large part of the incident power because of the shadow effect of particles and the thermal energy required for powder heating and melting.

Fig. 11b shows that the effective power available for the substrate is lower when the laser speed is decreased. This is mainly due to a larger quantity of power absorbed to melt the Ni particles. It is then coherent that the bonding clad-substrate is improved when laser speed increases (Fig. 4). The high degree of dilution observed by Ming et al. [4] with the increase of the scanning speed on low carbon steel AISI 1020 is probably due to the same phenomenum. A higher power is available at the substrate surface when the laser moves quickly since less powder has to be melted. Similar results have been found by Riveiro et al. [15]. This is obviously in

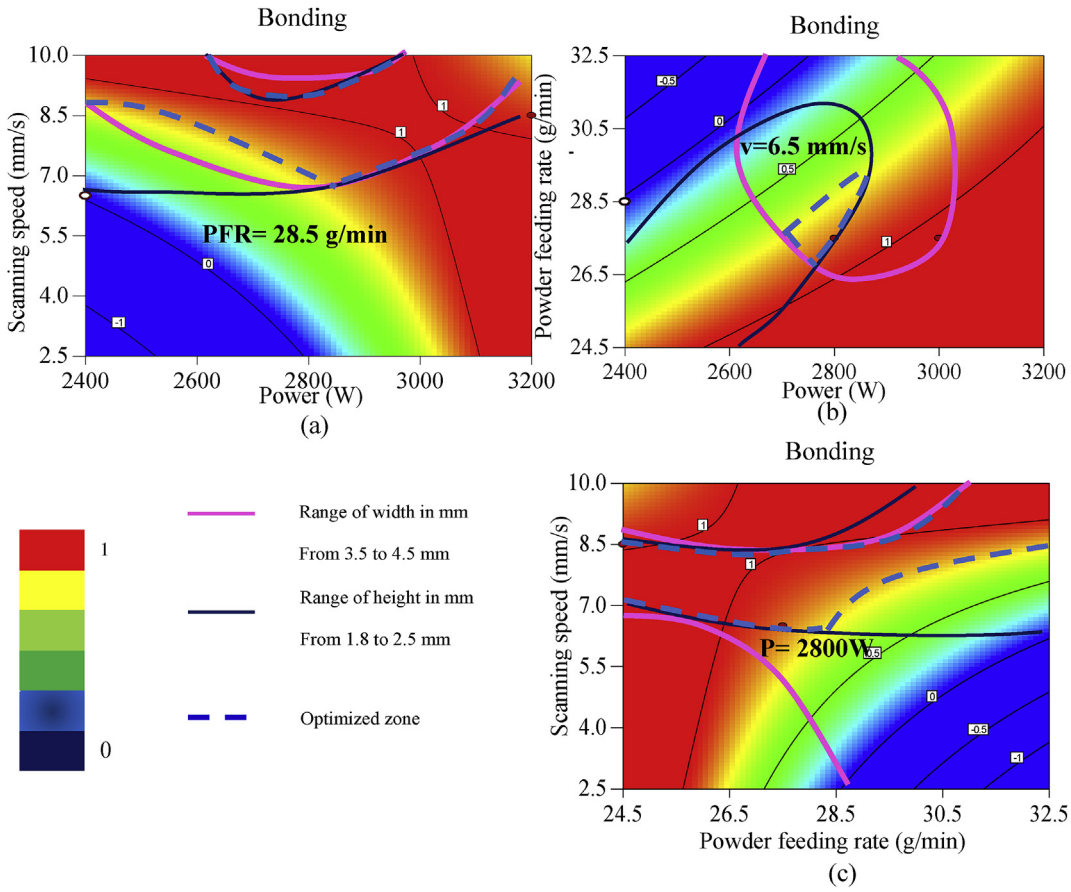

Fig. 8. Optimization of the process parameters. Bonding evolution with (a) the scanning speed (mm/s) and the power (W) for a fixed value of PFR at 28.5 g/min, (b) the PFR (g/min) and the power (W) for a fixed value of scanning speed at 6.5 mm/s and (c) the scanning speed (mm/s) and the PFR (g/min) for a fixed value of power at 2800 W. The attended optimized parameters are included into the dotted blue domains. (For interpretation of the references to colour in this figure legend, the reader is referred to the Web version of this article.)

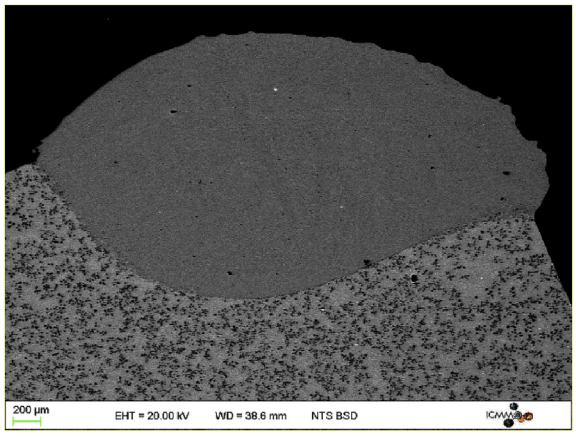

Fig. 9. SEM-BSE analysis of an optimized geometry and bonding (power 2800 W, scanning speed 8.5 mm/s and PFR of 27.5 g/min).

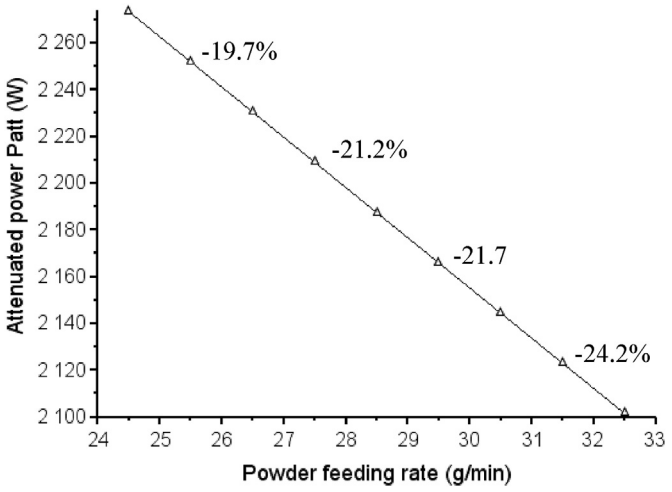

Fig. 10. Attenuated power versus PFR for a 2800 W incident laser power and associated K_{att} percentage.

contradiction with what is classically reported in SLM (selective laser melting) where an increase of laser speed scanning will induce a lack of heat input for powder fusion. Indeed, it is worth to be noted that in such processing conditions the thickness of powder to be melted is independent of the scanning speed [16]. On the contrary, in the present case of laser cladding, when the scanning speed is increased, the powder thickness is decreased.

Coupling these calculations with ANOVA simulation, it is possible to estimate the power, necessary at the substrate surface for bonding, P^{b}_{sub}, at different initial PFR. Indeed, the ANOVA model of bonding can give us the necessary initial power for bonding, P^{b}_{i}, for different PFR (bonding level = 1 in Fig. 8). The associated

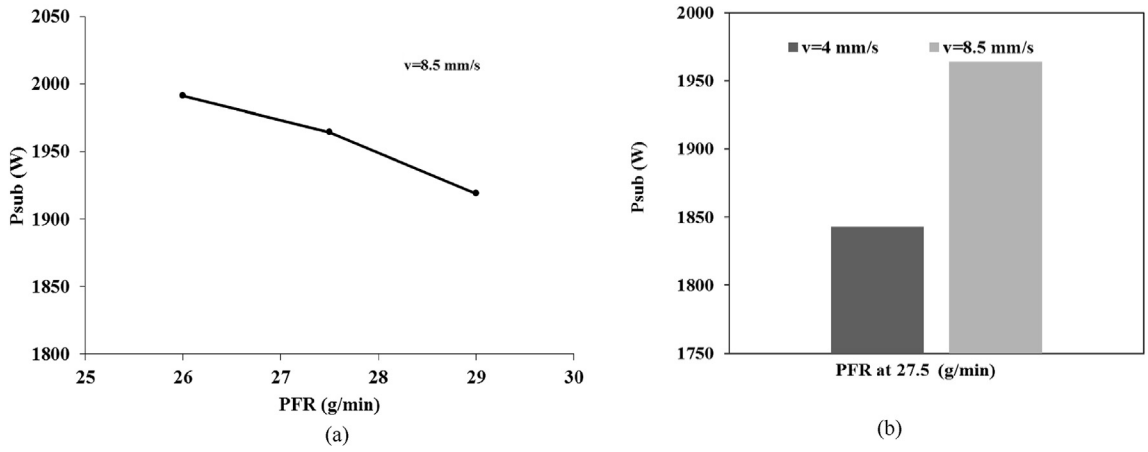

Fig. 11. Power at the substrate level for a given incident power of 2800 W a) as a function of PFR for a given scanning speed of 8.5 mm/s and b) for 2 scanning speeds at 27.5 g/min.

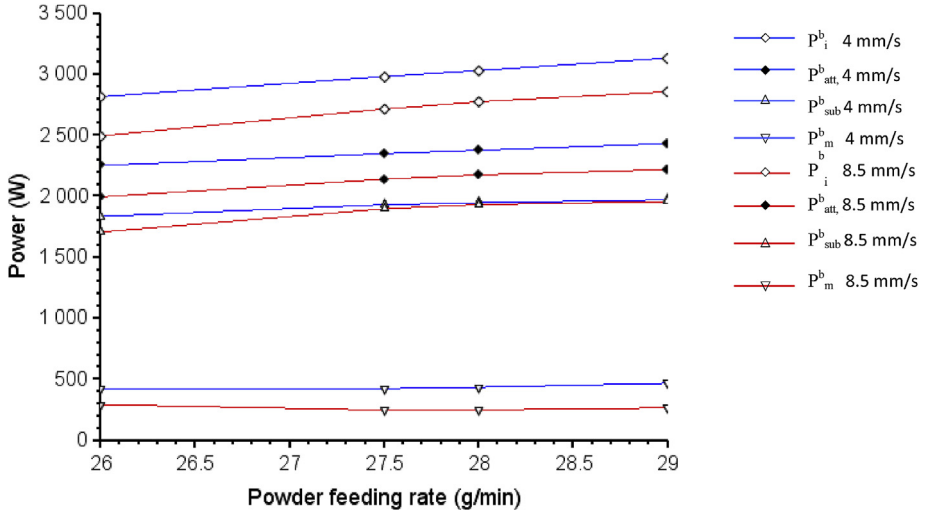

Fig. 12. Powers needed to guaranty a good bonding (level = 1) vs powder feeding rate (PFR). P^b_i, P^b_{att}, P^b_m, P^b_{sub} are the initial, attenuated, melting and substrate power needed for bonding, respectively, for two laser scanning speeds of 4 and 8.5 mm/s.

attenuated power, $P^b_{att,}$ available after the laser-powder interaction is then calculated, as well as the power needed for powder melting, P^b_m and are reported in a single graph (Fig. 12), for PFR values framing the optimized PFR of 27.5 g/min and for two scanning speeds of 4 and 8.5 mm/s.

Fig. 12 shows that, to get a good bonding, it is necessary to increase the initial power when the powder feeding rate increases, because of both the shadow effect and melting process even if this last one does not evolve much with PFR. In the same manner, at a low speed, the initial power must be important to ensure the bonding, because more power is needed for melting (around 400 W at 4 mm/s against 300 W at 8.5 mm/s) (Fig. 12). Once these two attenuation parts (shadow and melting) are subtracted to the initial power, it is interesting to note that the P^b_{sub}, necessary for bonding, is the same, whatever the scanning speed is (taking into account the measurement errors). P^b_{sub} is included in the range [1700–2000W] for the PFR values studied here [26–29 g/min]. This may constitute the power threshold that the Cu-Ni-Al substrate must receive in order to allow the perfect clad bonding.

Besides, a chemical dilution between the Ni clad and the Cu-Ni-Al substrate has been measured by EDS analysis after cladding over 40 μm all along the interface cladding/substrate (Fig. 2a). This thin layer may correspond to a fusion zone at the substrate surface [15]. To melt this layer, a power of about 10 W is sufficient in the scanning speed studied. Then, it is clear that P^b_{sub} (1700–2000W) is largely overestimated. Several reasons may be at the origin of the gap. First, in the calculation of P_m, it has been assumed that the maximum temperature (T_{max}) reached by the Ni based powder does not exceed the melting point. This assumption underestimates P_m but at this stage of the study no temperature measurements or finite element calculations have been performed to determine T_{max}. Furthermore, it is known that C_p evolves with temperature [9], but in the present work, C_p has been considered as constant in the entire range of temperatures up to T_m. This also contributes to the underestimate P_m. Consequently, the calculated P^b_{sub} is overestimated. To get an estimation of this error, it is possible, in first approximation, to calculate the power need to heat the molten Ni up to $T_{max} = 2200$ K similar to that found by finite element method by Peyre et al. in TA6V [9] with a mean specific heat of the liquid Ni of 1.5.C_p. From these assumptions, P_m would increase from 300 W to about 500 W for 8.5 mm/s. A high power still remains at the substrate.

Second, a large part of P^b_{sub} is in fact reflected by the substrate [13] since the Cu-Ni-Al absorptivity is low (0.06). Thus, it only

remains 0.06 of this P^{b}_{sub} (a few dozen watts) to ensure the chemical dilution and as a consequence the bonding. For low absorptivity substrates, such as Cu-Ni-Al alloy, it is then not surprising that high initial laser powers (2800 W in the present case) are required to provide a clad junction without delamination defects.

It has to be mentioned that the powder grain size and the powder distribution have significant effects on the power attenuation. Tabernero et al. [12] have observed that the decrease of the particle size induces an increase of the power attenuation (Eq. (7)). Also, the powder distribution needs to be mentioned since it is modified according to the substrate position in relation to the powder focal plane. In our case, the substrate is placed at the focal plane of the powder stream, so, a Gaussian distribution is observed. This can, under certain conditions, lead to a lack of bonding at the center of the powder flow.

5. Conclusion

Laser cladding of Ni-powder has been performed on a curved surface of a Cu-Ni-Al alloy. The current study consisted in building a statistical analysis based on response surface methodology to predict the clad geometry as well as the bonding quality with the substrate. The following conclusions have been highlighted:

- The height and width decrease when the speed increases because at high speed the amount of powder available for melting is lower.
- The increase of laser scanning speed and the decrease of the PFR improve the bonding. This can be explained by two effects: (i) when the PFR decreases, less powder conducts to reduce the Ni-particles shadow and thus lets more incident power go through the laser-powder interaction area down to the substrate, and (ii) when the scanning speed increases or PFR decreases, less energy is used for the powder melting and thus the substrate receives more power. Dilution between Ni coating and substrate is then possible and ensures a good bonding quality.

Optimized process parameters (PFR of 27.5 g/min, power of 2800 W and scanning speed of 8.5 mm/s) allowing both the perfect bonding and the desired clad dimensions, have been determined using an ANOVA approach and were confirmed by experimental results. This study demonstrated the efficacy of using the Taguchi and ANOVA method to obtain the optimal process conditions for laser cladding.

Using ANOVA results, the calculation of the attenuated power has been possible, as well as the determination of the minimum power necessary to ensure an accurate clad/substrate bonding. This value is independent of the laser scanning speed and nearly independent of the PFR. Knowing this threshold value, and the evolutions of intermediate attenuation rates (shadow and melting) as a function of scanning speed and PFR, it is possible to calculate the incident power necessary to get an effective cladding.

Acknowledgments

Authors want to thank C. Adoub, N. Barbosa and C. Lafarge from the CHPOLANSKY establishments for their help in the samples elaboration by laser cladding and their great skills about this technology applied to non-planar surfaces. This research was supported by the ANRT (French National Agency for Research and Technology) and the CHPOLANSKY establishments.

References

[1] W.M. Steen, J. Mazumder, Laser Material Processing, fourth ed., Springer, 2010.
[2] M. Rege, S. Van Linden, Stage de formation aux techniques de rechargement dans l'industrie verrière, Etablissements CHPOLANSKY, 2016.
[3] C.M. Lin, Parameter optimization of laser cladding process and resulting microstructure for the repair of tenon on steam turbine blade, Vacuum 115 (2015) 117–123, https://doi.org/10.1016/j.vacuum.2015.02.021.
[4] Q. Ming, L.C. Lim, Z.D. Chenc, Laser cladding of nickel-based hardfacing alloys, Surf. Coating. Technol. 106 (1998) 174–182.
[5] A.A. Moosa, M.J. Kadhim, A.D. Subhi, Dilution effect during laser cladding of inconel 617 with Ni-Al powders, Mod. Appl. Sci. 5 (2011) 50–55.
[6] Y. Sun, M. Hao, Statistical analysis and optimization of process parameters in Ti6Al4V laser cladding using Nd:YAG laser, Optic Laser. Eng. 50 (2012) 985–995, https://doi.org/10.1016/j.optlaseng.2012.01.018.
[7] U. de Oliveira, V. Ocelík, J.T.M. De Hosson, Analysis of coaxial laser cladding processing conditions, Surf. Coating. Technol. 197 (2005) 127–136, https://doi.org/10.1016/j.surfcoat.2004.06.029.
[8] V. Ocelík, U. de Oliveira, M. de Boer, J.T.M. de Hosson, Thick Co-based coating on cast iron by side laser cladding: analysis of processing conditions and coating properties, Surf. Coating. Technol. 201 (2007) 5875–5883, https://doi.org/10.1016/j.surfcoat.2006.10.044.
[9] P. Peyre, P. Aubry, R. Fabbro, R. Neveu, A. Longuet, Analytical and numerical modelling of the direct metal deposition laser process, J. Phys. D Appl. Phys. 41 (2008) 1–10, https://doi.org/10.1088/0022-3727/41/2/025403.
[10] R. Sabre, Plans d'expériences - Méthode de Taguchi, Tech. l'ingénieur. F1006, 2014, pp. 1–4.
[11] D. Chessel, A.B. Dufour, Fiche de Biostatistique Analyses de la variance, Biométrie Biol. Evol. Univ. Lyon 1 (2003) 1–31.
[12] I. Tabernero, A. Lamikiz, S. Martínez, E. Ukar, L.N. López De Lacalle, Modelling of energy attenuation due to powder flow-laser beam interaction during laser cladding process, J. Mater. Process. Technol. 212 (2012) 516–522, https://doi.org/10.1016/j.jmatprotec.2011.10.019.
[13] F. Wirth, D. Eisenbarth, K. Wegener, Absorptivity measurements and heat source modeling to simulate laser cladding, Phys. Procedia. 83 (2016) 1424–1434, https://doi.org/10.1016/j.phpro.2016.08.148.
[14] P. Peyre, Les Procédés Laser, PIMM, Arts Metiers Paris Tech, 2014, pp. 1–97. https://docplayer.fr/13824487-P-peyre-pimm-arts-et-metiers-paristech.html.
[15] A. Riveiro, A. Mejias, F. Lusquinos, J. Del Val, R. Comesana, J. Pardo, J. Pou, Optimization of laser cladding for Al coating production, Phys. Procedia. 41 (2013) 327–334, https://doi.org/10.1016/j.phpro.2013.03.085.
[16] C. Kusuma, S.H. Ahmed, A. Mian, R. Srinivasan, Effect of laser power and scan speed on melt pool characteristics of commercially pure titanium (CP-Ti), J. Mater. Eng. Perform. 26 (7) (2017) 3560–3568.